

Electromagnetics-Based RIS Channel Model with Near-Field Accuracy Improvement

Franek, Ondrej

Published in:
18th European Conference on Antennas and Propagation, EuCAP 2024

DOI (link to publication from Publisher):
[10.23919/EuCAP60739.2024.10501004](https://doi.org/10.23919/EuCAP60739.2024.10501004)

Publication date:
2024

Document Version
Accepted author manuscript, peer reviewed version

[Link to publication from Aalborg University](#)

Citation for published version (APA):
Franek, O. (2024). Electromagnetics-Based RIS Channel Model with Near-Field Accuracy Improvement. In *18th European Conference on Antennas and Propagation, EuCAP 2024* IEEE (Institute of Electrical and Electronics Engineers). <https://doi.org/10.23919/EuCAP60739.2024.10501004>

General rights

Copyright and moral rights for the publications made accessible in the public portal are retained by the authors and/or other copyright owners and it is a condition of accessing publications that users recognise and abide by the legal requirements associated with these rights.

- Users may download and print one copy of any publication from the public portal for the purpose of private study or research.
- You may not further distribute the material or use it for any profit-making activity or commercial gain
- You may freely distribute the URL identifying the publication in the public portal -

Take down policy

If you believe that this document breaches copyright please contact us at vbn@aub.aau.dk providing details, and we will remove access to the work immediately and investigate your claim.

Electromagnetics-Based RIS Channel Model with Near-Field Accuracy Improvement

Ondrej Franek^{*§}

^{*}APMS Section, Department of Electronic Systems, Aalborg University, Aalborg, Denmark, of@es.aau.dk

[§]Department of Radio Electronics, Brno University of Technology, Brno, Czechia

Abstract—An enhanced electromagnetics-based channel model of communication between two devices via reconfigurable intelligent surface (RIS) that enables closer placement of the devices to the RIS is described. This improvement is achieved by decomposing the communication paths between the RIS and the devices into individual paths for each RIS element. Key features include the use of commercial simulation software for device characterization, physical-level modeling of RIS inter-element coupling, fast device linking using the scattering matrix formalism, and easy emulation of fading or blockage. The model is implemented as a MATLAB function and additionally offers higher-order interpolation for improved accuracy.

Index Terms—Reconfigurable intelligent surfaces, electromagnetics, propagation.

I. INTRODUCTION

A Reconfigurable Intelligent Surface (RIS) is an emerging technology in wireless communications that is designed to improve wireless communication efficiency, enhance signal coverage, and mitigate interference in wireless networks, including future generations such as 6G [1]. An RIS is a device that consists of a large number of programmable scattering elements. These devices are intended to be strategically placed in the environment, such as on walls, ceilings, or other surfaces. The RIS unit can adjust the phase and amplitude of the electromagnetic (EM) waves scattered off these elements, and by doing so, it can manipulate and optimize the propagation of wireless signals. RIS can be used to enhance the coverage of wireless networks, improve data rates and reduce dropped calls. It can also help in reducing interference and unintended exposure to electromagnetic fields in crowded environments [2].

To study and analyze the impact of RIS on wireless communications, several physics-compliant channel models incorporating RIS have been proposed [3]–[8]. Physics-compliant models describe the interactions between RIS elements and other objects in the environment using EM fields and waves, and can thus capture the physics of how RIS affects signal propagation, reflection, and scattering. More recently, there has been growing interest in realistically describing RIS using impedance (or admittance) matrices [9]–[15] and scattering parameters [13]–[16]. These models mostly focus at finding useful bounds on channel performance containing RIS rather than on providing methods how to include actual electromagnetic models of RIS and both end devices in the channel simulation. To avoid employing lengthy EM simulations, various

approximations are often introduced that eventually make the models questionable in terms of accuracy and generality.

In our recent article [17], we proposed a channel model that employs full-wave simulations to characterize the RIS on the physical level without resorting to too many approximations, correctly modeling the EM coupling between the RIS elements and allowing for arbitrary incidence and scattering angles. The model is based on characterization of each involved device, the transmitter (TX), the receiver (RX), and the RIS, by their radiation and scattering properties. The devices are then linked using planar EM waves propagating in free space between the devices.

Unfortunately, the assumption that the EM waves traveling between the three devices are planar is the main disadvantage of our previous model. As well-known from antenna theory, EM waves radiated or scattered from an object can be considered as planar (with acceptable error) only beyond a far-field distance

$$d > 2D^2/\lambda \quad (1)$$

dependent on wavelength λ and maximum geometrical dimension of the object D [18]. For our model, this rule implies that the distances between the devices must fulfil the far-field condition. Since RIS is a passive structure, its size must be large to have a significant effect, and this in turn means larger far-field distance. Validity of our previous model is thus limited to larger distances between RIS and the two other devices.

In this paper, we propose a new formulation of our model published in [17] that allows the TX and RX to be placed closer to RIS, as the radiative near-field performance of the model is improved. This is enabled by decomposition of the communication path to and from RIS into N individual paths addressing each of the N elements of RIS separately. At the same time, the number of simulations needed for building the model stays the same, because the radiation and scattering properties of the elements are derived from the radiation and scattering properties of the RIS as a whole. All advantages of the channel model are preserved, in particular:

- 1) The model utilizes off-the-shelf commercial software to characterize the involved devices by simulations.
- 2) Coupling between the RIS elements is modeled on the EM level and its accuracy stems from the simulation software.

- 3) The number of simulations is limited to reasonable levels, since the characterization of the devices is limited to plane-wave radiation and scattering.
- 4) Linking of TX, RX, and RIS is fast thanks to using the scattering matrix formalism.
- 5) Fading or blockage can be easily emulated by assigning arbitrary complex weights to the plane-wave propagation paths between the devices.

Similarly to the previous version described in [17], the new channel model is implemented as a function in Matlab [19] that takes Cartesian coordinates of TX and RX, and complex weights of the paths between the devices as input arguments, and provides the scattering or impedance matrix of the whole system as the output. In addition, the new version allows for higher-order interpolation of the radiation and scattering patterns characterizing the devices, which brings further improvements in accuracy of the resulting matrix. The proposed channel model aims to be a useful tool to study and analyze the impact of RIS on wireless communication channels, and thus to provide valuable insight for understanding the benefits and limitations of RIS technology.

II. THE CHANNEL MODEL

In this section, the overall principle of the proposed RIS-assisted channel model will be briefly reviewed. For detailed explanation, the reader is referred to [17].

Each of the three devices, TX, RX, and RIS, is separately simulated in EM simulation software to obtain its characterization in terms of incoming and outgoing planar EM waves. By consecutively feeding each of the antenna ports of the particular device by an incoming wave, we obtain the columns of the port scattering matrix \mathbf{S} where each row corresponds to an outgoing wave from the particular port. From the same simulations we further obtain radiation patterns in the form of columns of matrix \mathbf{H} where each row represents radiation of the device in a particular direction. To make the characterization complete, we consecutively illuminate the device with plane waves from several directions, to obtain the columns of the plane wave scattering matrix $\mathbf{\Sigma}$ where each row represents scattering of the device in a particular direction. The directions of illumination and observation are chosen to be in a rectangular grid in spherical coordinates.

The characterization as described above is performed beforehand, and the three matrices are stored in a file. The Matlab function loads the precomputed matrices, reduces them to contain only the elements corresponding to directions relevant to the user-defined positions of the TX, RX, and RIS in space (see Fig. 1), and collects them into system matrices

$$\mathbf{S}_{\text{sys}} = \text{blkdiag}(\mathbf{S}_{\text{TX}}, \mathbf{S}_{\text{RX}}, \mathbf{S}_{\text{RIS}}) \quad (2)$$

$$\mathbf{H}_{\text{sys}} = \text{blkdiag}(\mathbf{H}_{\text{TX}}, \mathbf{H}_{\text{RX}}, \mathbf{H}_{\text{RIS}}) \quad (3)$$

$$\mathbf{\Sigma}_{\text{sys}} = \text{blkdiag}(\mathbf{\Sigma}_{\text{TX}}, \mathbf{\Sigma}_{\text{RX}}, \mathbf{\Sigma}_{\text{RIS}}) \quad (4)$$

where $\text{blkdiag}()$ denotes block diagonal matrix. Finally, the total scattering matrix of the entire system is calculated

$$\mathbf{S}_{\text{tot}} = \mathbf{S}_{\text{sys}} + \mathbf{H}_{\text{sys}}^{\text{T}} (\mathbf{C}^{-1} - \mathbf{\Sigma}_{\text{sys}})^{-1} \mathbf{H}_{\text{sys}} \quad (5)$$

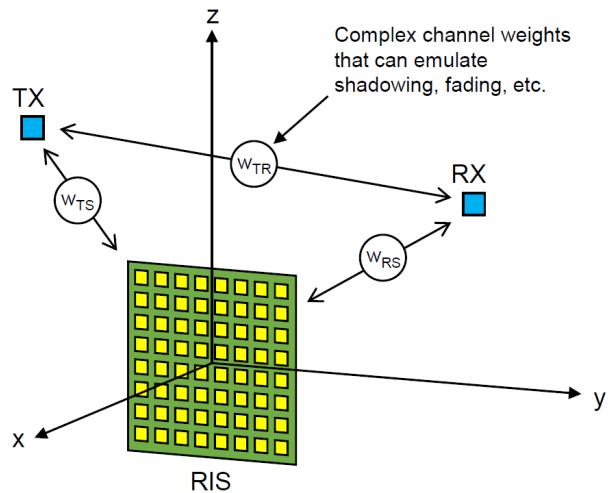


Fig. 1. The proposed electromagnetics-based model [17]: The RIS is placed at the origin of coordinates with its normal in the x -direction, TX and RX can be placed at arbitrary positions; The 3 devices are characterized by EM simulations and linked via EM plane waves using arbitrary complex weights w_{TR} , w_{TS} , and w_{RS} .

where \mathbf{C} is a connector matrix containing free space path losses between the three devices, possibly multiplied by user-defined complex weights.

III. NEAR-FIELD ACCURACY IMPROVEMENT

The original model as described in [17] and reviewed in the previous section is accurate only if the three devices are positioned in distances beyond the far field limit (1). In our case, the dominating structure is the RIS due to its inherently large electrical size. For typical RIS that has a form of a planar rectangular array with $M \times M = N$ elements and with $\lambda/2$ spacing between the elements, the far-field distance given by (1) is $N\lambda$. For smaller distances, the contributions of the RIS elements are burdened by too large phase errors due to differences in path lengths [18].

To improve the near-field performance of the model, we chose to treat each RIS element as a separate entity with its own path to TX and RX, but without the need to separately characterize each of the RIS elements (see Fig. 2), which would be extremely time-consuming. Instead, we reuse the EM simulations of the entire RIS and 1) apply appropriate phase shifts to the elements of the radiation matrix \mathbf{H} and scattering matrix $\mathbf{\Sigma}$, and 2) use correct path lengths from the RIS elements to TX and RX in the connector matrix \mathbf{C} . These two steps are explained in the following subsections.

A. Element phase shifts

Let us assume that $\mathbf{r}_i = (x_i, y_i, z_i)$ is the position vector of i -th RIS element, and similarly $\mathbf{r}_{\text{TX}} = (x_{\text{TX}}, y_{\text{TX}}, z_{\text{TX}})$ and $\mathbf{r}_{\text{RX}} = (x_{\text{RX}}, y_{\text{RX}}, z_{\text{RX}})$ are position vectors of TX and RX, respectively. The precomputed RIS radiation matrix \mathbf{H}_{RIS} is reduced not to 2 directions as in the previous model, but to $2N$ directions given by vectors $\mathbf{r}_i^{(\text{TS})} = \mathbf{r}_{\text{TX}} - \mathbf{r}_i$ and

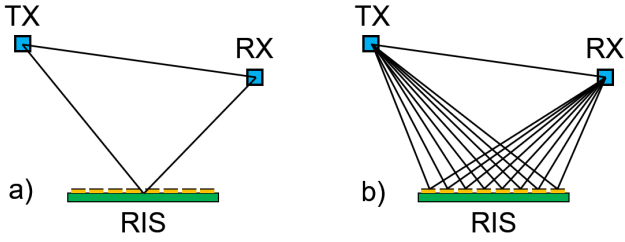


Fig. 2. Principle of the proposed near field accuracy improvement: a) previous version [17], in which RIS was treated as one entity and the propagation paths were terminated at its geometrical center; b) proposed version, where each RIS element has its own path towards TX and RX, but their EM characterization is still derived from the entire RIS.

$\mathbf{r}_i^{(RS)} = \mathbf{r}_{RX} - \mathbf{r}_i$. Two complex coefficients are created to perform the phase shift of the RIS element with respect to the origin of coordinates for which the RIS was characterized:

$$g_i^{(TS)} = \exp(-jk\mathbf{r}_i^{(TS)} \cdot \mathbf{r}_i / \|\mathbf{r}_i^{(TS)}\|) \quad (6)$$

$$g_i^{(RS)} = \exp(-jk\mathbf{r}_i^{(RS)} \cdot \mathbf{r}_i / \|\mathbf{r}_i^{(RS)}\|) \quad (7)$$

These two coefficients are then instrumental in forming two radiation vectors:

$$\left(\mathbf{H}_{RIS}^{(TS)}\right)_i = g_i^{(TS)} \mathbf{H}_{RIS}(\mathbf{r}_i^{(TS)}, i) \quad (8)$$

$$\left(\mathbf{H}_{RIS}^{(RS)}\right)_i = g_i^{(RS)} \mathbf{H}_{RIS}(\mathbf{r}_i^{(RS)}, i) \quad (9)$$

where the two arguments of the \mathbf{H}_{RIS} matrix are the radiation direction (row) and RIS element index (column), and the complex coefficients $g_i^{(\cdot)}$ add the phase shifts caused by displacement of the i -th RIS element. The two radiation vectors are now utilized to construct the reduced radiation matrix

$$\mathbf{H}'_{RIS} = \begin{bmatrix} \text{diag}(\mathbf{H}_{RIS}^{(TS)}) \\ \text{diag}(\mathbf{H}_{RIS}^{(RS)}) \end{bmatrix} \quad (10)$$

which is then inserted into (3) in place of \mathbf{H}_{RIS} .

Similar procedure is taken to construct the scattering matrix. Three scattering vectors are formed as

$$\left(\boldsymbol{\Sigma}_{RIS}^{(TST)}\right)_i = \left(g_i^{(TS)}\right)^2 \boldsymbol{\Sigma}_{RIS}(\mathbf{r}_i^{(TS)}, \mathbf{r}_i^{(TS)})/N \quad (11)$$

$$\left(\boldsymbol{\Sigma}_{RIS}^{(RST)}\right)_i = g_i^{(TS)} g_i^{(RS)} \boldsymbol{\Sigma}_{RIS}(\mathbf{r}_i^{(TS)}, \mathbf{r}_i^{(RS)})/N \quad (12)$$

$$\left(\boldsymbol{\Sigma}_{RIS}^{(RSR)}\right)_i = \left(g_i^{(RS)}\right)^2 \boldsymbol{\Sigma}_{RIS}(\mathbf{r}_i^{(RS)}, \mathbf{r}_i^{(RS)})/N \quad (13)$$

where the two arguments of the $\boldsymbol{\Sigma}_{RIS}$ matrix are the scattering direction (row) and illumination direction (column), and the complex coefficients again add the phase shifts caused by displacement of the i -th RIS element, here with double effect due to incoming and outgoing wave. In addition, the expressions are divided by N since each RIS element now acts as a separate scatterer with proportionally smaller scattering cross-section. The three scattering vectors are now used to construct the reduced scattering matrix

$$\boldsymbol{\Sigma}'_{RIS} = \begin{bmatrix} \text{diag}(\boldsymbol{\Sigma}_{RIS}^{(TST)}) & \text{diag}(\boldsymbol{\Sigma}_{RIS}^{(RST)}) \\ \text{diag}(\boldsymbol{\Sigma}_{RIS}^{(RST)}) & \text{diag}(\boldsymbol{\Sigma}_{RIS}^{(RSR)}) \end{bmatrix} \quad (14)$$

which is then inserted into (4) in place of $\boldsymbol{\Sigma}_{RIS}$.

B. Correct path lengths

Change of the endpoints of the paths need to be reflected also in the path loss terms that enter into the connector matrix \mathbf{C} . The free-space path loss vectors for TX-RIS and RX-RIS paths are defined, respectively,

$$\left(\mathbf{F}^{(TS)}\right)_i = \frac{j e^{-jk\|\mathbf{r}_i^{(TS)}\|}}{\lambda \|\mathbf{r}_i^{(TS)}\|} \quad (15)$$

$$\left(\mathbf{F}^{(RS)}\right)_i = \frac{j e^{-jk\|\mathbf{r}_i^{(RS)}\|}}{\lambda \|\mathbf{r}_i^{(RS)}\|} \quad (16)$$

and the free-space path loss term between TX and RX is defined [20]

$$F^{(TR)} = \frac{j e^{-jk r_{TR}}}{\lambda r_{TR}} \quad (17)$$

The path loss matrix \mathbf{F} is assembled using the complex weights as

$$\mathbf{F} = \text{diag}\left(w_{TR} F^{(TR)}, w_{TS} \mathbf{F}^{(TS)}, w_{RS} \mathbf{F}^{(RS)}\right) \quad (18)$$

and inserted into the connector matrix

$$\mathbf{C} = \begin{bmatrix} \mathbf{0} & \mathbf{F} \\ \mathbf{F} & \mathbf{0} \end{bmatrix} \quad (19)$$

The connector matrix \mathbf{C} is then used in (5) to obtain the total scattering matrix of the system of the three devices as observed from the ports of TX and RX.

IV. IMPLEMENTATION

The proposed model is implemented in the same way as the previous model described in [17], with CST Microwave Studio [21] as the simulation engine, and Matlab [19] for the wrapper function and all matrix manipulation. However, the EM characterizations can be performed in any simulation software that supports plane wave excitation, near-to-far-field transformation, and expression of S-parameters.

The syntax of the Matlab function is

```
M = ris_matrix( type, filename, ...
               x_TX, y_TX, z_TX, ...
               x_RX, y_RX, z_RX, ...
               w_TR, w_TS, w_RS, ...
               interp_method )
```

where \mathbf{M} is the resulting scattering (\mathbf{S}_{tot}) or impedance (\mathbf{Z}_{tot}) matrix of the entire model. The arguments are the same as in [17], with the addition of the `interp_method` argument, that allows for different methods of interpolation between the directional samples of the \mathbf{H} and $\boldsymbol{\Sigma}$ matrices. Our experiments showed that higher-order interpolation (`cubic`, `spline`) offer slightly improved accuracy compared to default `linear`.

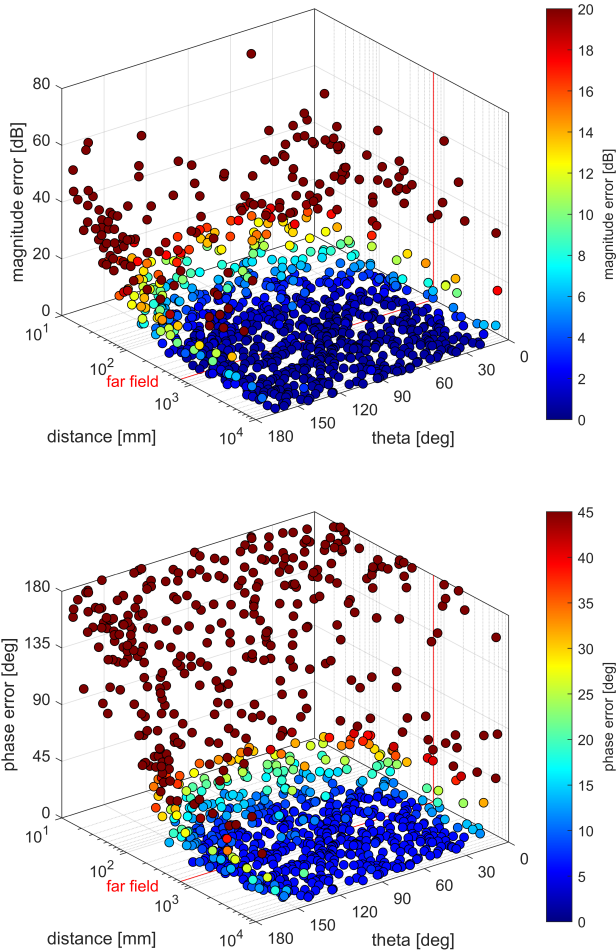


Fig. 3. Maximum magnitude (top) and phase (bottom) error in degrees across all elements of the scattering matrix \mathbf{S}_{tot} between the proposed model and full simulation, for a set of 1000 random positions of RX in front of the RIS; the red line denotes the far field limit of the RIS.

V. VALIDATION

The proposed improved channel model has been validated against full simulation in CST Microwave Studio [21] at frequency 28 GHz. The RIS is an 8×8 planar array of thin dipoles with length $0.93\lambda/2$ and radius $\lambda/500$, with the dipoles distributed in a rectangular grid with $\lambda/2$ spacing. The RIS is equipped with a rectangular perfectly conducting reflector with size $4.5\lambda \times 4.5\lambda$ at a distance of $\lambda/4$ behind the dipoles. The TX and RX are also dipoles with the same parameters as the RIS elements, all oriented in the z direction. The RIS is centered at coordinates $(0, 0, 0)$ facing the x direction, the TX is positioned at coordinates $(4, 3, 2)$ m, and RX is successively positioned at 1000 random points in the frontal hemisphere of the RIS. The RX positions are distributed uniformly in θ and ϕ spherical coordinates and logarithmically in distance from 10 mm to 10 m.

Figure 3 shows the magnitude and phase errors, respectively, between the proposed model and full simulation, taken as

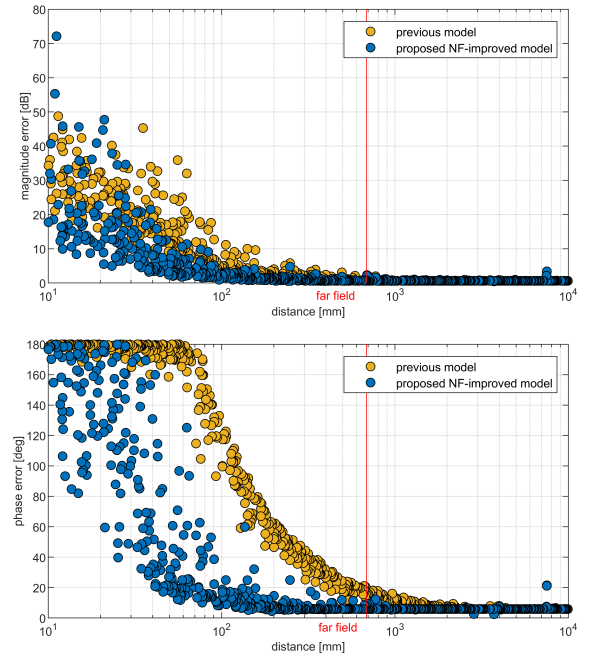


Fig. 4. Maximum magnitude (top) and phase (bottom) error in dB across all elements of the scattering matrix \mathbf{S}_{tot} for the previous and the proposed near-field-improved model with respect to full simulation, for a set of 1000 random positions of RX in front of the RIS; the red line denotes the far field limit of the RIS.

maximum values across all elements of the \mathbf{S}_{tot} matrix. The magnitude and phase errors are within approx. 2 dB and 10 degrees, respectively, in the central parts of the plots. The errors start growing significantly below approximately 200 mm, which is less than a third of the far field limit at 685 mm, and shows improved performance in the near field region. The errors also grow toward the upward ($\theta = 0^\circ$) and downward ($\theta = 180^\circ$) directions, since in these regions the coupling between the RIS and RX becomes weak due to the z -axis orientation of all the dipoles.

Figure 4 shows the magnitude and phase errors, respectively, when the points with $\theta \leq 30^\circ$ and $\theta \geq 150^\circ$ are disregarded, and offers a comparison between the previous model and the improved one. From this figure it should be apparent that the improved model indeed offers more accurate results when the RX approaches the RIS.

However, observation of Figs. 3–4 reveals a difficulty of comparing S-parameters with their magnitude and phase errors: the dB and phase errors tend to be gradually larger for smaller magnitudes of the S-parameters due to inherent noise. This is a common phenomenon affecting only the comparison of the two datasets and is not a limitation of the model whatsoever. To take a different look at the comparison, Fig. 5 shows the root-mean-square error (RMSE) and the absolute value error of the total scattering matrix with respect to full simulation, as an envelope taken from the farthest to the closest points. It is evident from the figure that the errors of the proposed model are up to $10\times$ lower with respect to the

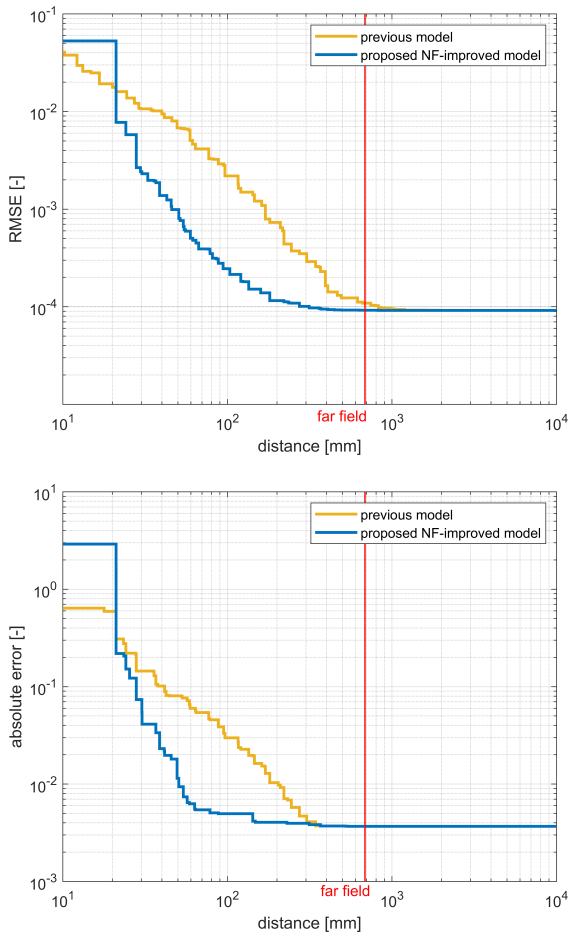


Fig. 5. Root-mean-square error (RMSE, top) and maximum absolute error across all elements (bottom) of the scattering matrix \mathbf{S}_{tot} for the previous and the proposed near-field-improved model with respect to full simulation, for a set of 1000 random positions of RX in front of the RIS; the red line denotes the far field limit of the RIS.

previous model, for distances down to approx. 20 mm, where the reactive near-field behavior starts affecting the results.

VI. CONCLUSION

We have introduced an improved channel model for communication between two end devices assisted by RIS, where each of the three devices is characterized based on their EM properties. The primary advantage of this model is its assumption that all radiated or scattered waves remain planar at the relevant distances, allowing for the utilization of readily available commercial simulation software to obtain the EM characteristics of these devices. Even though such assumption usually limits the validity of the model to far field distances, we have successfully demonstrated that by applying a slight modification to the procedure while using the same EM data the accuracy in near field can be significantly improved.

ACKNOWLEDGMENT

This work has been supported by the EU Horizon 2020 project RISE-6G.

- [1] E. Basar, M. Di Renzo, J. De Rosny, M. Debbah, M.-S. Alouini, and R. Zhang, "Wireless communications through reconfigurable intelligent surfaces," *IEEE Access*, vol. 7, pp. 116 753–116 773, 2019.
- [2] E. C. Strinati, G. C. Alexandropoulos, V. Sciancalepore, M. Di Renzo, H. Wymeersch, D.-T. Phan-Huy, M. Crozzoli, R. d'Errico, E. De Carvalho, P. Popovski *et al.*, "Wireless environment as a service enabled by reconfigurable intelligent surfaces: The RISE-6G perspective," in *2021 Joint European Conference on Networks and Communications & 6G Summit (EuCNC/6G Summit)*. IEEE, 2021, pp. 562–567.
- [3] M. Najafi, V. Jamali, R. Schober, and H. V. Poor, "Physics-based modeling and scalable optimization of large intelligent reflecting surfaces," *IEEE Trans. Commun.*, vol. 69, no. 4, pp. 2673–2691, 2020.
- [4] W. Tang, M. Z. Chen, X. Chen, J. Y. Dai, Y. Han, M. Di Renzo, Y. Zeng, S. Jin, Q. Cheng, and T. J. Cui, "Wireless communications with reconfigurable intelligent surface: Path loss modeling and experimental measurement," *IEEE Trans. Wireless Commun.*, vol. 20, no. 1, pp. 421–439, 2020.
- [5] F. H. Danufane, M. Di Renzo, J. De Rosny, and S. Tretyakov, "On the path-loss of reconfigurable intelligent surfaces: An approach based on Green's theorem applied to vector fields," *IEEE Trans. Commun.*, vol. 69, no. 8, pp. 5573–5592, 2021.
- [6] F. Costa and M. Borgese, "Electromagnetic model of reflective intelligent surfaces," *IEEE Open J. Commun. Soc.*, vol. 2, pp. 1577–1589, 2021.
- [7] R. Faqiri, C. Saigre-Tardif, G. C. Alexandropoulos, N. Shlezinger, M. F. Imani, and P. del Hougne, "PhysFad: Physics-based end-to-end channel modeling of RIS-parametrized environments with adjustable fading," *IEEE Trans. Wireless Commun.*, vol. 22, no. 1, pp. 580–595, 2022.
- [8] H. Prod'homme and P. del Hougne, "Efficient computation of physics-compliant channel realizations for (rich-scattering) RIS-parametrized radio environments," *IEEE Commun. Lett.*, 2023.
- [9] G. Gradoni and M. Di Renzo, "End-to-end mutual coupling aware communication model for reconfigurable intelligent surfaces: An electromagnetic-compliant approach based on mutual impedances," *IEEE Wireless Commun. Lett.*, vol. 10, no. 5, pp. 938–942, 2021.
- [10] P. Mursia, S. Phang, V. Sciancalepore, G. Gradoni, and M. Di Renzo, "Saris: Scattering aware reconfigurable intelligent surface model and optimization for complex propagation channels," *IEEE Wireless Commun. Lett.*, 2023.
- [11] K. Konno, S. Terranova, Q. Chen, and G. Gradoni, "Generalised impedance model of wireless links assisted by reconfigurable intelligent surfaces," *arXiv preprint arXiv:2306.03761*, 2023.
- [12] D. Badheka, J. Sapis, S. R. Khosravirad, and H. Viswanathan, "Accurate modeling of intelligent reflecting surface for communication systems," *IEEE Trans. Wireless Commun.*, 2023.
- [13] J. A. Nosseck, D. Semmler, M. Joham, and W. Utschick, "Physically consistent modelling of wireless links with reconfigurable intelligent surfaces using multiport network analysis," *arXiv preprint arXiv:2308.12223*, 2023.
- [14] M. Nerini, S. Shen, H. Li, M. Di Renzo, and B. Clerckx, "A universal framework for multiport network analysis of reconfigurable intelligent surfaces," *arXiv preprint arXiv:2311.10561*, 2023.
- [15] A. Abrardo, A. Toccafondi, and M. Di Renzo, "Design of reconfigurable intelligent surfaces by using s-parameter multiport network theory—optimization and full-wave validation," *arXiv preprint arXiv:2311.06648*, 2023.
- [16] S. Shen, B. Clerckx, and R. Murch, "Modeling and architecture design of reconfigurable intelligent surfaces using scattering parameter network analysis," *IEEE Trans. Wireless Commun.*, vol. 21, no. 2, pp. 1229–1243, 2021.
- [17] O. Franek, "Electromagnetics-based channel model of reconfigurable intelligent surfaces," in *2023 17th European Conference on Antennas and Propagation (EuCAP)*. IEEE, 2023, pp. 1–4.
- [18] C. A. Balanis, *Antenna Theory: Analysis and Design*. John Wiley & Sons, 2015.
- [19] "Matlab," <https://se.mathworks.com/products/matlab.html>, accessed: 2022-10-12.
- [20] O. Franek, "Phasor alternatives to Friis' transmission equation," *IEEE Antennas and Wireless Propag. Lett.*, vol. 17, no. 1, pp. 90–93, 2017.
- [21] "CST Studio Suite," <https://www.3ds.com/products-services/simulia/products/cst-studio-suite/>, accessed: 2022-10-12.